**JP4.9**

# OBSERVATIONS OF VELOCITY VARIANCE IN THE STABLE BOUNDARY LAYER

Dean Vickers* and L. Mahrt
Oregon State University, Corvallis, OR, U.S.A.

## 1. INTRODUCTION

Current atmospheric models under-represent mesoscale motions in the stable boundary layer. Such motions have been referred to as meandering, although the source of these motions is usually not clear. Mesoscale motions in the stable boundary layer include internal gravity waves, pulsating drainage flows, vortical modes or fossil turbulence, wake vortices and others (Mahrt et al., 2001 and references theirin). The physics responsible for generating such motions is not in the models. For example, the model removes motions through use of periodic boundary conditions and explicit filters that remove vertically propogating gravity waves.

Unresolved motions need to be parameterized. For example, if a plume model is driven with 1-h average wind components, all wind velocity fluctuations on timescales less than 1-h hour must be parameterized. Such fluctuations include turbulence and mesoscale motions. While the turbulence has been studied extensively and is currently parameterized in the models, the mesoscale motions are less well known and are typically not included in models.

We partition the observed variance into turbulence and mesoscale components, where mesoscale refers to scales larger than turbulence but less than 4 hours. Turbulence scales, identified from cospectra of the heat flux, vary from tens of seconds to several minutes depending on the mean wind speed and stratification (Vickers and Mahrt, 2003). The turbulence regime is associated with a velocity aspect ratio ($\sigma_w/\sigma_u$) near unity and high correlation between w and u and w and T. In the mesoscale regime, $\sigma_w/\sigma_u$ decreases with increasing scale.

The partitioning of the variance is performed because the physics responsible for the fluctuations is very different, and their influence on the plume is very different (e.g., Seinfeld, 1975). Turbulence is dispersive and dilutes the plume, while the longer timescale mesoscale motions primarily advect the plume. In a time-averaged sense, the mesoscale motions are "dispersive" in that they can reduce the concentration of a tracer at a point in space.

* *corresponding author address:* Dean Vickers, College of Oceanic and Atmospheric Sciences, Oregon State University, Corvallis, OR; *email*: vickers@coas.oregonstate.edu

In this study, we examine observations of the cross-wind velocity variance in the stable boundary layer to document the timescale, stability and height dependence. The variance at turbulence scales is contrasted with previous studies. The variance at mesoscales is examined for predictability and potential scaling relationships. Eight different tower datasets are used to test the generality of the results. The long-term goal is to provide improved formulations of dispersion.

## 2. DATA

The observations consist of high frequency measurements of the three wind velocity components and the temperature using 3-d sonic anemometers. The first four datasets include surfaces of short grass and bushes, snow and water. These include: a) the Cooperative Atmosphere-Surface Exchange Study (CASES-99) over Kansas, U.S.A. grassland in October 1999, b) the FLuxes Over Snow Surfaces Experiment (FLOSS) over rangeland in the North Park region of Colorado, U.S.A. during the winter of 2002-2003, c) a snow covered, treeless, flat coastal area near Barrow, Alaska during the spring of 2005, and d) an offshore Air-Sea Interaction Tower (ASIT) located 3 km south of Martha's Vineyard, Massachusets, U.S.A. during the summer of 2003, as part of the Coupled Boundary Layers Air Sea Transfer experiment (CBLAST Weak Wind).

CASES-99 and FLOSS data were collected by the Atmospheric Technology Division of the National Center for Atmospheric Research. The Alaska data were collected by Matthew Sturm (USA-CRREL-Alaska), and the ASIT data by Jim Edson (University of Connecticut).

The height of the sonic anemometer measurements is 5 m above ground in CASES-99 and FLOSS, 2.5 m above snow in Alaska and approximately 5 m above the ocean in CBLAST. The sampling rate was 20 hz for each experiment. The CASES-99 dataset includes seven different towers located within a circular region of radius 300 m.

The FLOSS tower is surrounded by high mountains with an east-west running Petersen ridge located a few kilometers upwind in the predominant flow direction (southerly). The grass surface in FLOSS ranged from snow covered to snow free during the 4 month experiment. Patches of short bushes protruding above the snow

were located a few hundred meters south of the tower and at scattered locations within the North Park region.

Three of the four remaining datasets are above tree canopies. These include: a) 3-m tall young ponderosa pine (YPine), b) 15-m tall mature ponderosa pine (MPine) with bush understory, and c) a 21-m tall aspen canopy in the boreal forest of Saskatchewan, Canada, during the spring and summer of 1994 (Aspen). The final dataset is from a recently burned region with a sparse stand of dead pine trees and grass understory (Burn). The three ponderosa pine sites are AmeriFlux sites in complex terrain in central Oregon, U.S.A. Twelve months of data are analyzed from 2004.

The YPine site was clear cut and replanted as an experimental research site in 1987, and the vegetation within the site is very homogeneous. The young pines occupy a region measuring 300 x 275 m with the tower approximately centered within the site. A stand of older and much taller pines surround the young site on all sides.

The sonic anemometers were located at 12 m at YPine (4 canopy heights), 10 m at Burn, 31 m at MPine (2 canopy heights) and 39 m (nearly 2 canopy heights) at the Aspen site. The YPine and MPine data were collected at 10 hz sampling while the Burn and Aspen data were collected at 20 hz. The semi-arid Oregon sites are characterized by sustained synoptic high pressure and weak large-scale flow in summer and fall

All datasets were processed with the same software. Raw time series were subjected to an automated quality control program to flag instrument problems. A tilt correction was applied to the 3-d wind components based on the wind direction dependence of the tilt angle averaged over the entire experiment. The horizontal wind components were rotated such that the 4-h average v-component was zero.

## 3. DECOMPOSITION

Multiresolution decomposition (Howell and Mahrt, 1997; Vickers and Mahrt, 2003) will be used to examine the scale-dependence of the velocity variance. Multiresolution analysis applied to time series decomposes the record into unweighted averages on dyadic time scales and represents the simplest possible orthogonal decomposition. In a dyadic sequence, each increasing scale is twice as large as the previous smaller one. The multiresolution basis set (Mallat, 1989) is a wavelet basis set, and is the only basis set that satisfies Reynold's averaging.

The variance is calculated for averaging time-scale $\tau$ as the sum of the orthogonal multiresolution modes from the smallest resolvable scale (2 data points) up to scale $\tau$. This summation of modes to obtain the variance (or covariance) is analogous to integration of the spectral density to obtain the variance using Fourier decomposition.

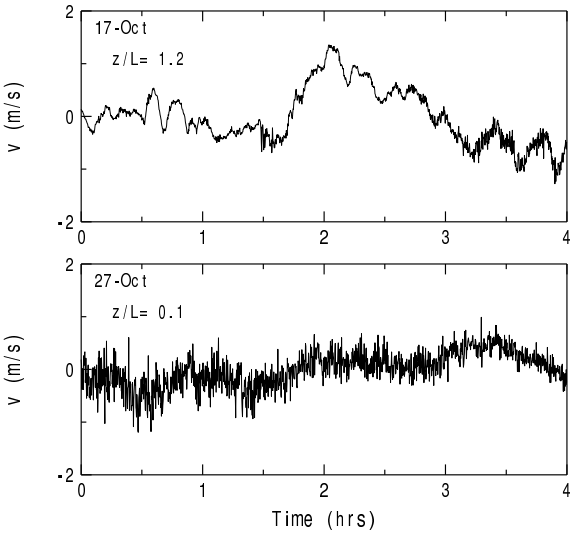


Figure 1: 4-h time series of the cross-wind velocity component for a stable case (top panel, 17-Oct) and a weakly stable case (bottom panel, 27-Oct) from CASES-99. Values have been averaged to 10-s for display purposes.

The multiresolution modes here are in kinematic units, such that the variance is equal to the sum, and not the integral, of the spectra.

Example time series of the cross-wind component for two different stability regimes are shown in Figure 1 with the corresponding spectra and variance in Figure 2. A gap region seperating turbulent motions from mesoscale motions is evident for both series (Figure 2). The gap is associated with a timescale of about 400 seconds for the weakly stable case and about 50 seconds for the more stable case. The variance at turbulence scales is suppressed about an order of magnitude associated with a factor of ten increase in $z/L$. The relative contribution to the variance from mesoscale motions is significant for the stable case, but negligible for the weakly stable one. The 4-h variance is the same for both records.

## 4. TIMESCALE DEPENDENCE

The cross-wind velocity variance ($v'^2$) increases with increasing averaging time at timescales less than 10 s due to the inclusion of more turbulence with increased averaging time (Figures 3 and 4). For a given averaging time, the variance is suppressed by stronger stability. A gap region in the velocity spectra between turbulence and mesoscale motions, when it occurs, is indicated where the variance levels off or increases more slowly with increasing averaging time. An active mesoscale region is indicated where the variance begins to again increase with increasing averaging time at scales larger than the

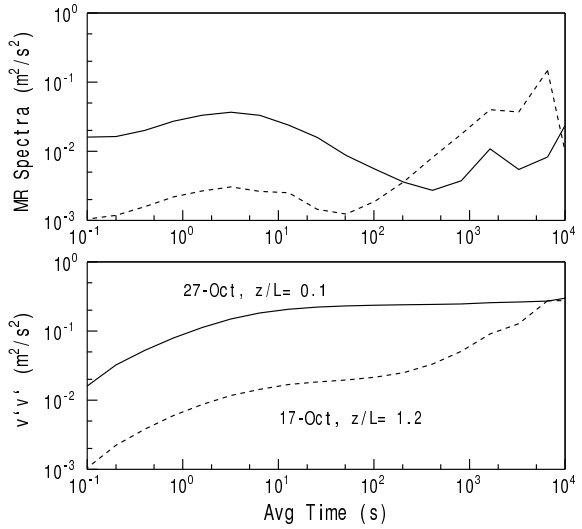


Figure 2: Multiresolution spectra (top panel) of the cross-wind velocity component for the time series in Figure 1 for the weakly stable case (solid) and the more stable case (dash). Bottom panel is the variance (sum of the orthogonal modes).

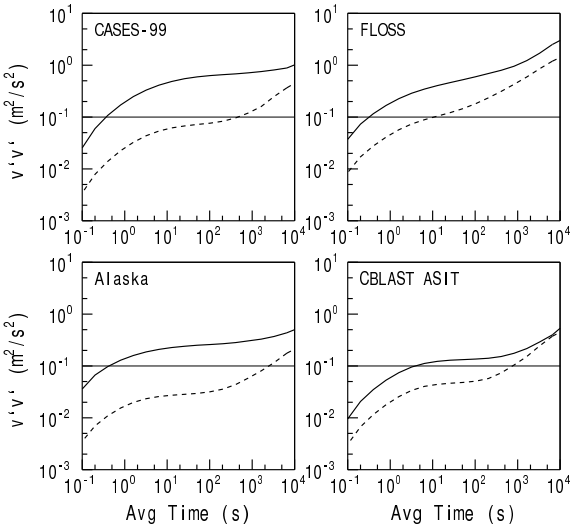


Figure 3: Composited cross-wind velocity variance for weakly stable ($0 < z/L < 0.1$, solid) and stable ($0.1 < z/L < 2$, dash) conditions. L is the Obukov length scale.

gap region. The gap region in $v'^2$ is less pronounced in the composites (Figures 3 and 4) compared to many examples of individual 4-h records because the timescale associated with the gap region varys significantly between records.

While the composites are smooth functions of averaging time, individual records exhibit a wide range of averaging time dependence and a wide range of values for a given stabliity class and averaging time (Figure 5). The between record variation of the variance, for a given averaging time and stability class, is an order of magnitude for FLOSS data. The largest skewness is found at turbulence scales ($\tau$ = 5 minute) in the stronger stability category.

## 5. NORMALIZED VARIANCE

Scaling the variance by the momemtum flux ($u_*^2$) essentially removes the stability-dependence of the averaging time dependence at turbulence scales (Figures 6 and 7). The maximum timescale where the scaling successfully collapses the data is related to the gap region seperating turbulence from mesoscale motions. This maximum timescale is about 100 s in the composites and varies slightly between sites.

The normalized velocity variance at mesoscales is substantially larger with stronger stability compared to weaker stability at all the sites (Figures 6 and 7). However, the increase in the normalized variance is more strongly related to the decrease in $u_*^2$ than it is to an in-

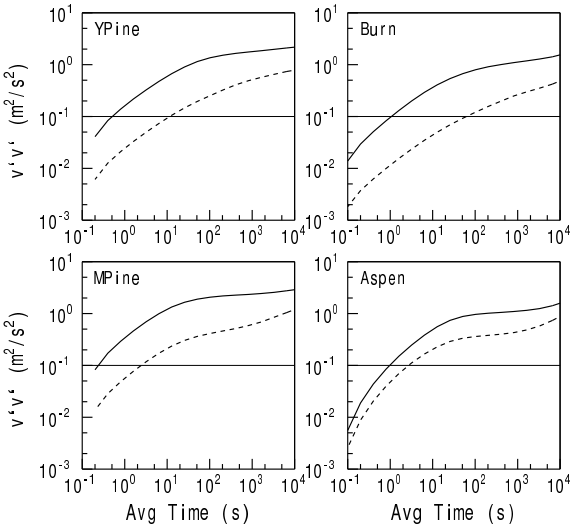


Figure 4: Same as Figure 3 except for different sites.

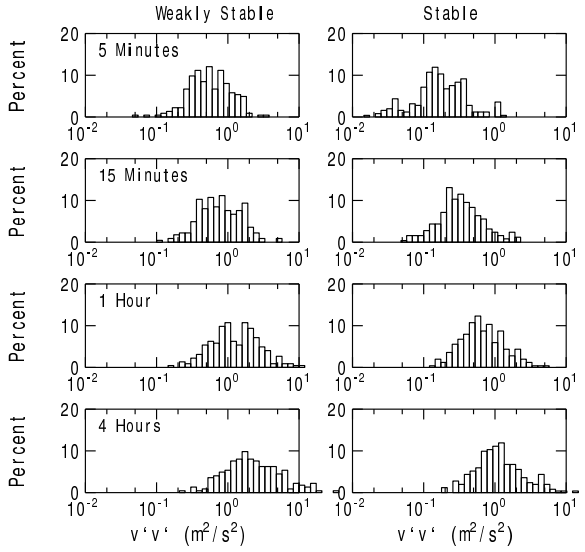


Figure 5: Frequency distribution (percent) of the cross-wind variance for weakly stable (left column) and stable (right column) conditions in FLOSS. Rows represent different averaging timescales.

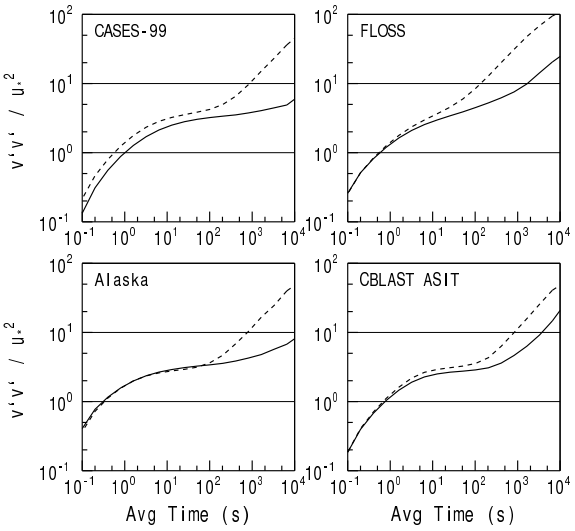


Figure 6: Scaled composited cross-wind velocity variance for weakly stable (solid) and stable (dash) conditions.

crease in $v'^2$, and the decrease in $u_*^2$ is in large part due to self-correlation since $z/L$ contains $u_*^3$. Therefore, the larger normalized velocity variance at mesoscales for the stronger stability cases does not indicate increased velocity variance.

Scaling the variance by the wind stress reduces the between record variations at turbulence scales in weak stability, but increases the between record variations at larger scales in strong stability (Figures 5 and 8, and Table 1). The above results show that meandering and other mesoscale motions should not be parameterized in terms of $u_*$. These results also indicate that universal spectra bridging the turbulence and mesoscale motions are not possible.

Table 1. Between-record standard deviation of the cross-wind velocity variance corresponding to the frequency distributions in Figure 5. Values in parenthesis are for the normalized velocity variance in Figure 8.

| $\tau$ | Weakly Stable | Stable |
|---|---|---|
| 5 m | 0.29 (0.16) | 0.36 (0.33) |
| 15 m | 0.30 (0.21) | 0.31 (0.44) |
| 1 h | 0.33 (0.28) | 0.30 (0.48) |
| 4 h | 0.38 (0.35) | 0.33 (0.50) |

## 6. HEIGHT DEPENDENCE

The multiple levels of sonic anemometers in the CASES-99 and FLOSS field programs are used to exam-

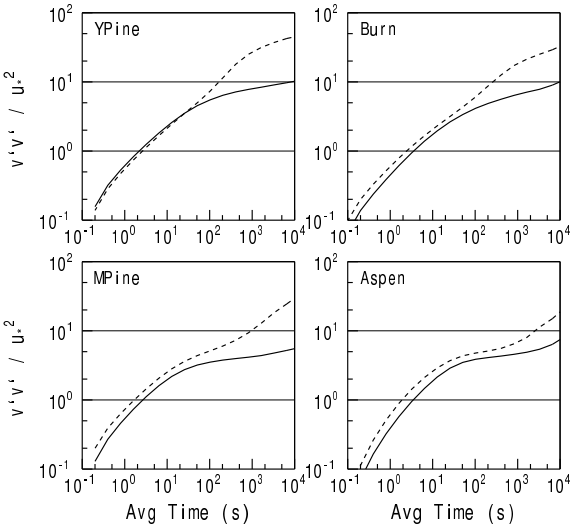


Figure 7: Same as Figure 6 except for different sites.

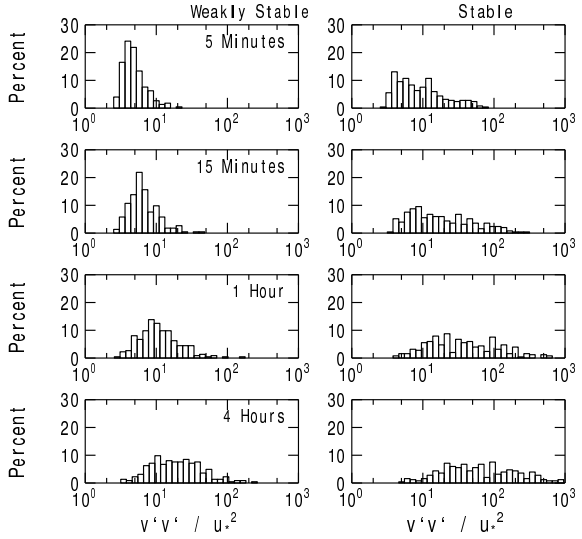


Figure 8: Frequency distribution (percent) of the normalized cross-wind variance for weakly stable (left column) and stable (right column) conditions in FLOSS. Rows represent different averaging timescales.

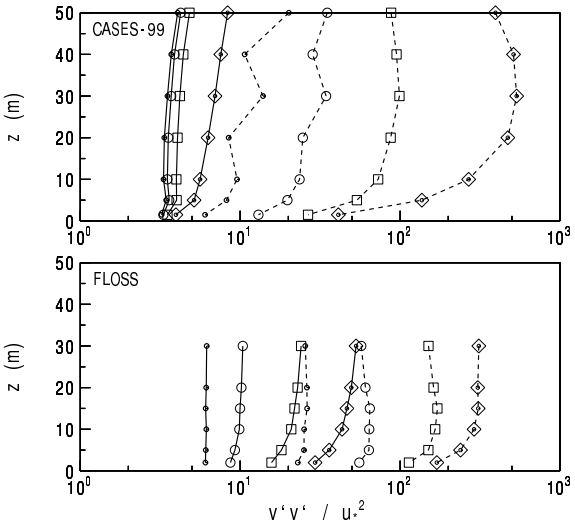


Figure 9: Composite height dependence of $v'^2/u_*^2$ for weakly stable ($0 < z/L < 0.1$, solid) and stable ($0.1 < z/L < 2$, dash) conditions for $\tau = 5$ min (dot), 15 min (circle), 1 h (square) and 4 h (diamond).

ine the height dependence of $v'^2/u_*^2$ (Figure 9). The composite structure is coherent in the vertical at both sites. There is a wide gap region for the CASES-99 weakly stable data at all levels, where $v'^2/u_*^2$ increases only slowly with increasing $\tau$. By contrast, $v'^2/u_*^2$ increases strongly with $\tau$ at all levels for the weakly stable FLOSS data where the gap region in $v'^2$ is often less pronounced or non-existent.

For the CASES-99 more stable data, $v'^2/u_*^2$ at large timescales increases rapidly with height in the lowest 20 m and then is relatively constant with height above this level. One interpretation is that the longer timescale (or low frequency) 2-d motions are more inhibited by the surface than the smaller scale motions. For FLOSS, the decrease near the surface is less dramatic but occurs for both weakly stable and stable conditions.

The $v'^2/u_*^2$ associated with only turbulence ($\tau = 5$ min in Figure 9), is nearly constant with height for the weakly stable category, and slightly increases with height for the stronger stability class. Smaller scale 2-d motions are less inhibited by the surface.

## 7. TURBULENCE SCALES

At turbulence scales, the standard deviation of the cross-wind component scales with the friction velocity (Figures 10 and 11), confirming most previous studies. The intercepts from the regressions in Figure 10 (0.06, 0.19, 0.03 and 0.08 m s$^{-1}$ for CASES-99, FLOSS, Alaska and ASIT, respectively), imply that some cross-wind variance survives even as the momentum flux approaches zero, possibly due to mesoscale variance captured within the averaging window. The intercepts are larger at the tall canopy sites (0.18, 0.13, 0.15 and 0.12 m s$^{-1}$ for YPine, Burn, MPine and Aspen, respectively).

Combining the eight datasets with equal weight, the average value of $\sigma_{vT}/u_*$ is 1.8 with a standard deviation of 0.22. The average value of the intercept ($\sigma_{vT}$ as $u_*$ approaches zero) is 0.12 m s$^{-1}$ with a standard deviation of 0.06 m s$^{-1}$. $\sigma_{vT}/u_*$ is 20% lower than the average for the marine boundary layer. The ASIT site has the smallest range of observed $u_*$ and the least amount of data. $\sigma_{vT}/u_*$ is 20% higher than average at the YPine site. The flow adjustment triggered by the large to small surface roughness change a few hundred meters upwind from the YPine tower may be a factor. The largest scatter (smallest $R^2$ value) in the $u_*$-$\sigma_{vT}$ relationship is found for FLOSS.

The American Meteorological Society and the U.S. Environmental Protection Agency regulatory dispersion model (AERMOD) (Cimorelli et al., 2005) specifies $\sigma_{vT}^2 = 3.6\, u_*^2$, equivalent to a slope of 1.9 in Figures 10 and 11, based on Panofsky and Dutton (1984) and Izumi (1971). Nasstrom et al. (1999) specify a slope of 2.06 in their real-time dispersion modeling system based on the work of Nieuwstadt (1985) and Lenschow et al. (1988), however, a minimum value of $\sigma_{vT}$ = 0.5 m s$^{-1}$ is used.

For weakly stable conditions with $z/L < 0.1$, where they found that $\sigma_{vT}/u_*$ was nearly independent of $z/L$,

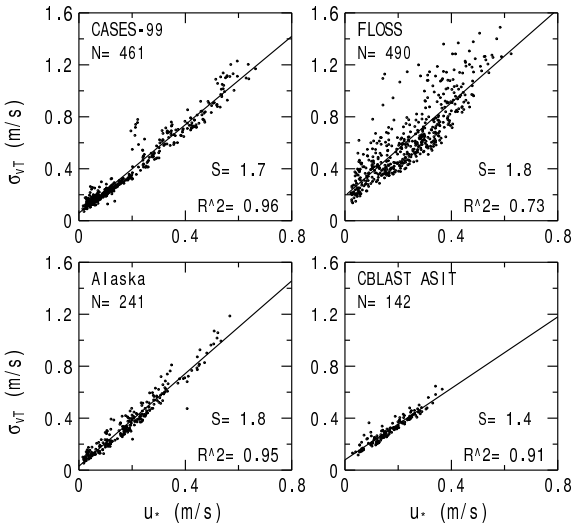


Figure 10: Standard deviation of the cross-wind component of the wind due to turbulence ($\sigma_{vT}$) as a function of friction velocity ($u_*$). N is the number of 4-h average stable records, S and $R^2$ are the the slope and variance explained by regression.

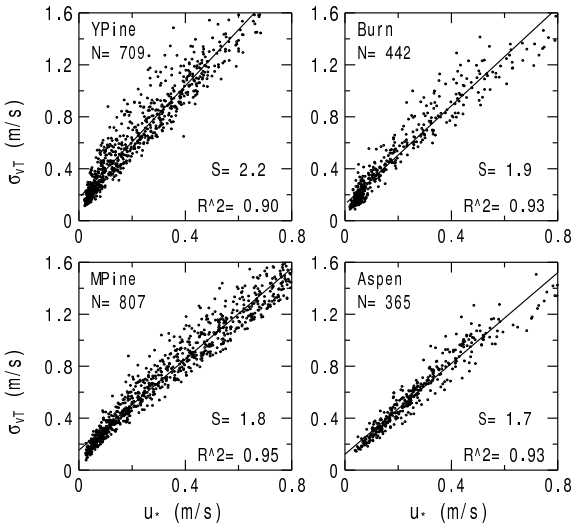


Figure 11: Same as Figure 10 except for different sites.

Pahlow et al. (2001) and Smedman (1988) reported the average value of $\sigma_{vT}/u_*$ to be 2.0 and 1.7,respectively. We choose the regression method to estimate an average value of $\sigma_{vT}/u_*$ because the method of averaging $\sigma_{vT}/u_*$ is potentially contaminated with self-correlation since z/L contains $u_*^3$. The strongest stability records in Figures 10 and 11 are concentrated near the origin.

The friction velocity and $\sigma_{vT}$ in Figures 10 and 11 are computed using a $\tau = 5$-minute timescale to define the turbulent fluctuations. An alternative method was also applied where the fluctuations are computed from a record dependent variable $\tau$ based on the spectral gap in the multiresolution heat flux cospectra (Vickers and Mahrt, 2006). Such an approach reduces the random flux error for strongly stable conditions for individual records by excluding poorly sampled mesoscale motions. The averaging time varies from tens of seconds for the weakest wind speed and most strongly stable records to several minutes for the strongest wind speed and weakly stratified records.

Using the alternate method, the slopes at the short canopy sites are slightly larger (1.7, 2.2, 1.9 and 1.5 for CASES-99, FLOSS, Alaska and ASIT, respectively), and the intercepts are smaller (0.03, 0.05, 0 and 0.06 m $s^{-1}$ for CASES-99, FLOSS, Alaska and ASIT, respectively). The alternate method also leads to slightly larger slopes compared to the fixed $\tau = 5$ min method for the tall canopy sites (2.4, 2.0, 1.8 and 1.8 for YPine, Burn, MPine and Aspen, respectively), and slightly smaller intercepts (0.08, 0.07, 0.12 and 0.11 for YPine, Burn, MPine and Aspen, respectively). The smaller intercepts result from the more effective removal of mesoscale motions by the variable averaging width method. Removal of the mesoscale motions is important because the dispersion efficiency of the mesoscale motions may be less than that for turbulence.

## 8. MESOSCALE VARIANCE

The contribution to the variance from mesoscale motions alone is computed as

$$\sigma_{vM}^2(\tau) = \sigma_v^2(\tau) - \sigma_{vT}^2 \qquad (1)$$

where $\sigma_v^2(\tau)$ is the total variance at timescale $\tau$ and $\sigma_{vT}^2$ is the variance due to turbulent motions. There are at least two different approaches that could be used for partitioning the variance. One is to include variance on all scales larger than the gap scale based on the heat flux cospectra. However, this redefines the small scale lower limit for the mesoscale calculation for each record depending on the turbulence. Such an approach could artificially force a dependence of $\sigma_{vM}$ on the turbulence. A second approach is to use a fixed small scale lower limit (e.g., 5 minutes). The drawback of this approach is that it can inadvertantly include small scale mesoscale motions in $\sigma_{vT}$. The 4-h $\sigma_{vM}$ is not sensitve to the method chosen (Figure 12), however, the sensitivity increases with decreasing $\tau$.

With the possible exception of drainage flows at Burn and MPine and topographic generation of waves at FLOSS (see below), $\sigma_{vM}$ in general does not scale with the friction velocity (Figures 13 and 14), the mean wind

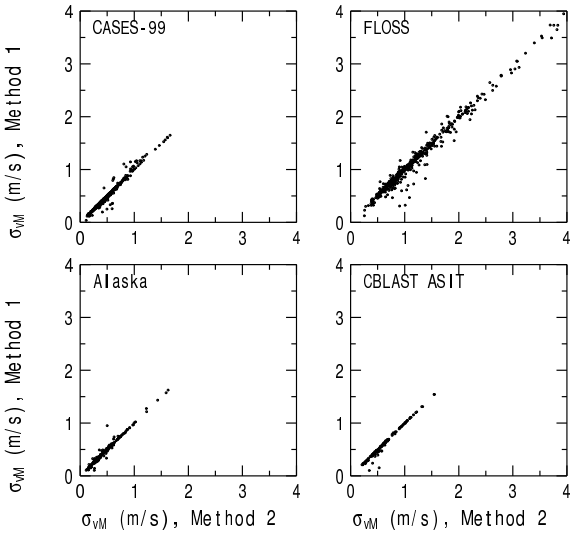


Figure 12: Standard deviation of the cross-wind component of the wind due to mesoscale motions ($\sigma_{vM}$) for $\tau = 4$ h for two different methods of defining the turbulence: 1 employs the variable gap scale based on the heat flux cospectra, and 2 uses a fixed 5-minute window.

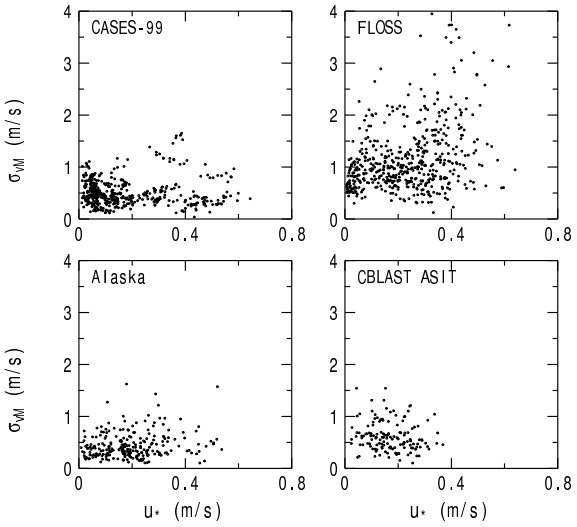


Figure 13: $\sigma_{vM}$) for $\tau = 4$ h as a function of friction velocity ($u_*$). $\sigma_{vT}$ calculated using variable $\tau$ based on heat flux cospectra..

speed (not shown) or $z/L$ (not shown). The mesoscale motions at the majority of sites are unpredictable in terms of the characteristics of the local mean flow or turbulence.

The general failure of $\sigma_{vM}$ to be related to $u_*$ suggests that coupling mechanisms between the two scales are not sufficiently strong to dominate. Such coupling might include intermittent shear-generation of turbulence due to fluctuations of shear associated with $\sigma_{vM}$, and increase of $\sigma_{vM}$ through collapsed turbulence, resulting two-dimensional motions and upscale energy transfer (e.g. vortex merging). Further examination of the potential importance of such mechanisms would require sophisticated analysis techniques and inclusion of the role of $\sigma_{uM}$.

At the Burn site, there are indications that the mesoscale variance may be reduced in well-defined drainage flows, although the scatter is large and the relationship may be circumstantial (Figure 15). In such flow, the stability ($z/L$) is enhanced and the mesoscale variance is suppressed. The less systematic drainage flows at the MPine site do not typically extend upward above the canopy to the 31-m level anemometer. However, additional measurements from a subcanopy flux system at 3 m height indicate some enhancement of stability and suppression of mesoscale velocity variance in drainage flows (Figure 16). The generality of this result to other drainage flow situations is not known. Because the stability and the existance of well-defined drainage flow are

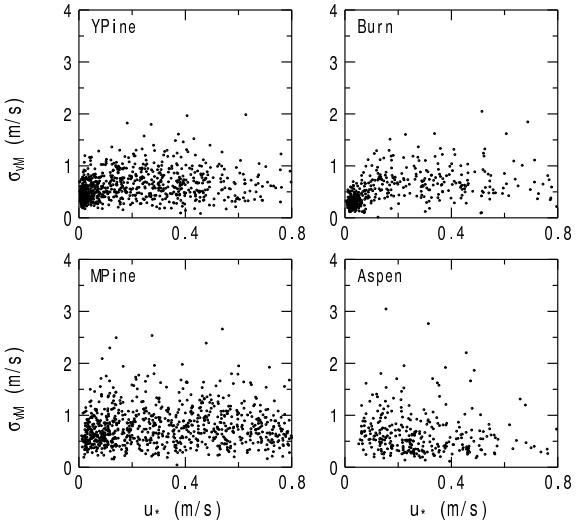


Figure 14: Same as Figure 13 except for different sites.

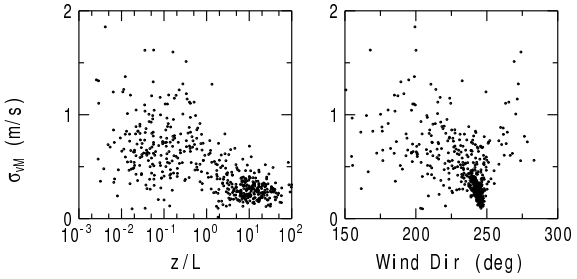


Figure 15: Burn site $\sigma_{vM}$ for $\tau = 4$ h as a function of stability ($z/L$) and wind direction. The drainage flow is from 245 degrees.

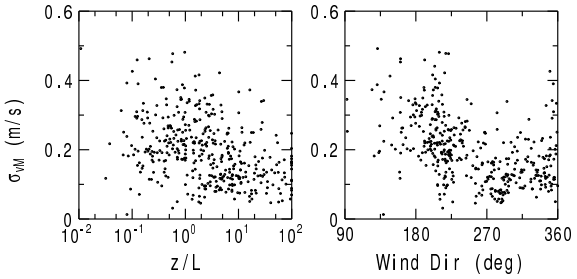


Figure 16: Same as Figure 15 except for 3-m subcanopy data from the MPine site, where the drainage flow is from the northwest.

strongly correlated at these two sites, it is difficult to identify whether the mechanism responsible for reducing the cross-wind variance is stability or drainage flow.

For FLOSS, there is a systematic increase in $\sigma_{vM}$ with increasing $u_*$ or wind speed, and with decreasing $z/L$ (Figure 17), although the scatter is large (Figure 13).. We speculate that topographic generation of 2-d motions by Petersen ridge is enhanced with stronger mean flow, and thus indirectly correlated with $u_*$.

## 9. AUTOCORRELATION FUNCTIONS

The autocorrelation function can provide information on how long mesoscale disturbances last before they disappear. In this section we document the time lag associated with the first zero-crossing of the autocorrelation function for v. Prior to computing the autocorrelations, the wind components are time averaged using 100-s block averaging to remove most of the turbulence scale fluctuations.

In general, the time lag increases with the scale of the disturbance. When the scale of the disturbance exceeds the record length (4 h), for example motions associated with larger scale diurnal or synoptic variations, the autocorrelation function stays positive for all lags and does not cross zero. For smaller scale wave type motions, the autocorrelation function always becomes negative.

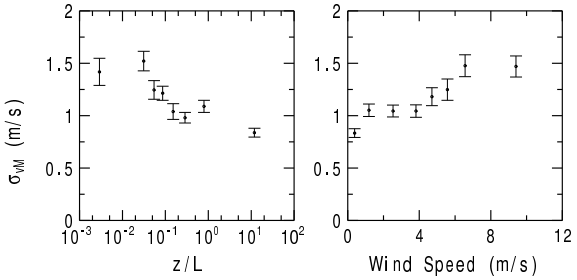


Figure 17: Bin-averaged FLOSS $\sigma_{vM}$ for $\tau = 4$ h as a function of stability ($z/L$) and wind speed. Each bin contains approximately 60 4-h data records. Error bars show $\pm$ one standard error about the mean for the bin.

The time lag associated with the first zero-crossing is not related to stability ($z/L$) or to the strength of the mesoscale fluctuations ($\sigma_{vM}$) (Figure 18). The shape of the autocorrelation function appears to be unpredictable based on local variables. The frequency distribution indicates a wide range of lag times with no preferred modes (Figure 19). Approximately 20% of the time in CASES-99 and 10% of the time in FLOSS, there is no zero-crossing. These records contain significant trend associated with larger scale changes in the mean wind direction.

## 10. SUMMARY

The scale-dependent cross-wind velocity variance at a particular site has large variation, even for a given stability class and scale. The between-site variation is generally less than the between-record variation at a given site, which can be an order of magnitude or more. Normalizing the scale-dependent variance by $u_*^2$ effectively removes the stability dependence at turbulence scales but does not at mesoscales. The larger $v'^2/u_*^2$ at mesoscales with strong stability compared to weak stability is primarily due to the decrease in $u_*^2$ not an increase in $v'^2$.

At turbulence scales, $v'^2/u_*^2$ is nearly constant with height in the lowest 30 to 50 m above ground during weakly stable conditions, and slightly increases with height in stronger stability. At mesoscales, $v'^2/u_*^2$ increases rapidly with height in the lowest 20 m and then is relatively constant with height up to 50 m. The larger scale 2-d motions appear to be more inhibited by the presence of the surface than the much smaller scale 3-d turbulennt motions.

The standard deviation of the cross-wind component due to turbulence ($\sigma_{vT}$) scales with the friction velocity,

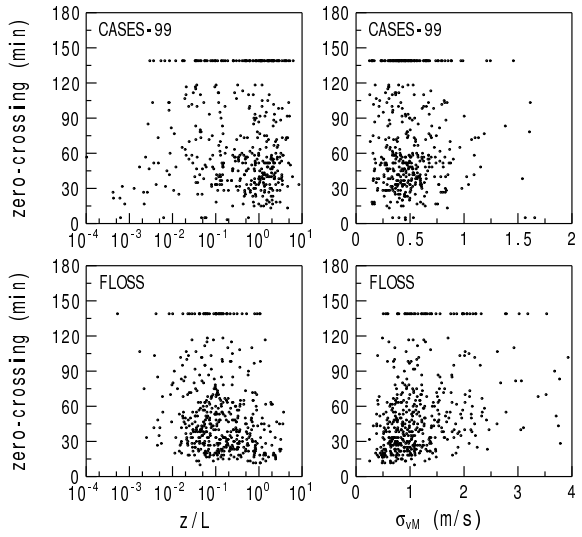


Figure 18: Time lag associated with the first zero-crossing of the autocorrelation function of the cross-wind component of the mean wind. The time lag is shown as a constant (140) for records where there is no zero-crossing.

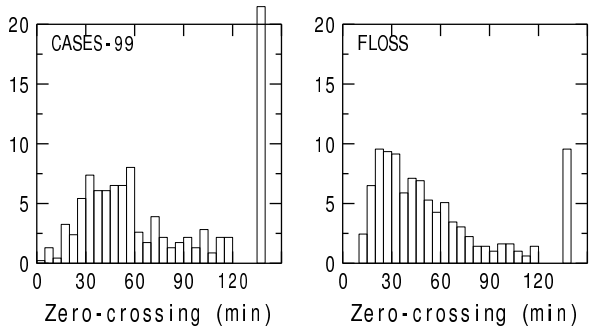


Figure 19: Frequency distribution (percent) of the time lag associated with the first zero-crossing of the autocorrelation function of the 100-s averaged cross-wind component of the mean wind. The percent of the records with no zero-crossing is shown on the far right.

as reported by numerous other studies. Considering eight different datasets, we find the average value of $\sigma_{vT}/u_*$ to be 1.8 with a standard deviation of 0.22. The average minimum value of $\sigma_{vT}$ as $u_*$ approaches zero is 0.12 m $s^{-1}$ with a standard deviation of 0.066 m $s^{-1}$. $R^2$ values from linear regression of $\sigma_{vT}$ against $u_*$ were greater than 0.9 for seven of the eight datasets.

The standard deviation of the cross-wind component due to mesoscale motions ($\sigma_{vM}$) generally does not scale with the friction velocity, wind speed or stability. In such cases, the mesoscale motions are unpredictable using local variables. Possible exceptions were found in drainage flow situations at complex terrain forested sites where $\sigma_{vM}$ was suppressed in the stronger stability conditions associated with well-defined drainage flows, and at the FLOSS site where topographic generation of 2-d motions appears to be enhanced in stronger winds (or weaker stability) due to the presence of an upstream ridge.

The time lag associated with the first zero-crossing of the autocorrelation function of v is not related to stability or to the magnitude of the mesoscale motions ($\sigma_{vM}$). The frequency distribution of the time lags shows a wide range of values that occur with nearly equal probability.

One conclusion is that fluctuations of the cross-wind component appear to be unpredicatble in terms of local variables, except possibly for some special situations like drainage flows. The mesoscale motions may originate elsewhere and propogate into the local area. Apparently, the coupling between the turbulence and such motions is weak. Detailed case studies of individual records may be the only path to further our understanding, however, if every night is a different case study with its own special features, progress will remain slow.

In the near future, we plan to study diffusion using a particle simulation technique with the CASES-99 network of towers.

## REFERENCES

Cimorelli,A.J., and coauthors, 2005, AERMOD: A dispersion model for industrial source applications. Part I: General model formulation and boundary layer characterization. *J. Appl. Meteor.*, 44, 682-693.

Howell,J.F., and L.Mahrt, 1997, Multiresolution flux decomposition. *Boundary-Layer Meteorol.*, 83, 117-137.

Izumi,Y., 1971, Kansas 1968 Field Program data report. Air Force Cambridge Research Laboratory, No. 379, AFCRL-72-0041, 79 pp.

Lenschow,D.H., X.Sheng Li, C.Jaun Zhu, and B.B.Stankov, 1988, The stably stratified boundary

layer over the Great Plains. *Boundary-Layer Meteorol.*, 42, 95-121.

Mahrt,L., E.Moore, D.Vickers, and N.O.Jensen, 2001, Dependence of turbulent and mesoscale velocity variances on scale and stability. *J. Appl. Meteor.*, 40, 628-641.

Mallat,S.G., 1989, The theory of multiresolution signal decomposition: the wavelet representation. *IEEE Trans. Pattern Anal. Machine Intell.*, 7, 674-693.

Nasstrom,J.S., G.Sugiyama, J.M.Leone,Jr., and D.L.Emak, 2000, A real-time atmospheric dispersion modeling system. Eleventh Joint Conference on the Applications of Air Pollution Meteorology with the Air and Waste Management Association, Preprint UCRL-JC-135120, Long Beach, CA, January 2000.

Nieuwstadt,F.T.M., 1985, A model for the stationary, stable boundary layer. Turbulence and diffusion in stable enviornments, J.C.R.Hunt, Ed., Clarendon Press, Oxford, pp 149-179.

Pahlow,M., M.B.Parlange, and F.Porte-Agel, 2001, On Monin-Obukov similarity in the stable atmospheric boundary layer. *Boundary-Layer Meteorol.*, 99, 225-248.

Panofsky,H.A., and J.A.Dutton, 1984, *Atmospheric Turbulence: Models and Methods for Engineering Applications*. John Wiley and Sons, 417 pp.

Seinfeld,J.H., 1975, *Air pollution: physical and chemical fundamentals*. McGraw-Hill, 523 pp.

Smedman,A.S., 1988, Observations of a multi-level turbulence structure in a very stable atmospheric boundary layer. *Boundary-Layer Meteorol.*, 44, 231-253.

Vickers,D., and L.Mahrt, 2003, The cospectral gap and turbulent flux calculations. *J. Atm. and Oc. Tech.*, 20, 660-672.

Vickers,D., and L.Mahrt, 2006, A solution for flux contamination by mesoscale motions with very weak turbulence. *Boundary-Layer Meteorol.*, in press.